GeoVirtual 2020 September 14-16
Resilience and Innovation

Effects of structure on the mechanical behavior of loess: implications for flowslides in cemented soils

Fangzhou Liu
Department of Civil and Environmental Engineering – University of Alberta, Edmonton, AB, Canada
J. David Frost & Jorge Macedo
School of Civil and Environmental Engineering – Georgia Institute of Technology, Atlanta, GA, USA
Qiang Xu
State Key Laboratory of Geohazard Prevention and Geoenvironment Protection – Chengdu University of Technology, Chengdu, Sichuan, China

ABSTRACT
Loess contains predominately silt-sized quartz grains that are bonded by various cementation agents, that is of significant interest to the understanding of the mechanical properties of lightly cemented soils. Loess is problematic upon wetting as its metastable structure can rapidly transform from a cemented solid body to a fluidized material. The results of series of isotropically consolidated undrained tests (CIU) compare the large-strain behaviors of intact and reconstituted specimens, that show state-dependent flow instability due to the effect of structure. A constitutive understanding is gained using NorSand model by comparing the computed undrained behaviors of intact and reconstituted loess at the same state parameter. The results confirms the strong effect of structure on flow instability. The drained-to-undrained transition in the loading path of loess is simulated, and indicates a rapid reduction in strength under such a transition for loess, thereby the triggering mechanism of loess flowslides.

RÉSUMÉ
Le loess contient principalement des grains de quartz de la taille d'un limon liés par divers agents de cimentation, ce qui présente un intérêt important pour la compréhension des propriétés mécaniques des sols légèrement cimentés. Le loess est problématique lors du mouillage car sa structure métastable peut rapidement se transformer d'un corps solide cimenté en un matériau fluidisé. Les résultats d'une série de tests non drainés (CIU) isotropiquement consolidés comparent les comportements à grande déformation d'échantillons intacts et reconstitués, qui montrent une instabilité de l'écoulement dépendante de l'état en raison de l'effet de la structure. Une compréhension constitutive est acquise à la lumière du modèle NorSand en comparant les comportements non drainés calculés de loess intact et reconstitué au même paramètre d'état. Les résultats confirment le fort effet de la structure sur l'instabilité de l'écoulement. La transition drainée à non drainée dans le chemin de chargement du loess est simulée, ce qui indique une réduction rapide de la résistance sous une telle transition pour le loess, et donc le mécanisme de déclenchement des coulées de flux de loess.

1 INTRODUCTION

Loess is typically a silt-sized soil, with a silt fraction of 70%-100%, that is bonded by various cementation agents, e.g. salt (Fan et al. 2017), water-film (Derbyshire and Mellors 1988, Pye 1995), carbonate (Milodowski et al. 2015), and clay (Smalley et al. 2006). Researchers are not unanimous about the origins of the interparticle bonds (Barden et al. 1973, Derbyshire et al. 1995, Delage et al. 1996, Jiang et al. 2012).

As a natural cemented soil, loess is problematic upon wetting as its meta-stable structure can rapidly transform from a cemented solid body to a fluidized material. In recent work, Peng et al. (2018) characterized more than 70 loess-related slope failures that were induced by irrigation on the Heifangtai terrace (HFT). The irrigation in HFT provides 4-6 cycles of groundwater recharge annually, which has increased the groundwater level by 20 m at an average rate of 0.18 m/yr and caused about 200 landslides along the margin of the terrace.

Qi et al. (2018) analyzed 20 multi-staged retrogressive loess flowslides that are medium- to large-scale slope failures with rapid movement and long runout exhibiting liquefied and fluidized flow behavior with failure surfaces developed entirely within the overlying loess layer. The mechanism of loess flowslides has been largely ascribed

to flow liquefaction which is characterized by the sudden loss of strength with the development of large strains accompanied by increasing pore water pressure under monotonic loading. The meta-stable structure appears to facilitate the onset of the 'flow-like' movement, as strong contractive responses with rapid decrease in strength are observed for intact silty loess (Zhou et al. 2014, Leng et al. 2018, Xu et al. 2018, Zhang and Wang 2018).

Liu et al. (2019) analyzed the flow behavior of the HFT loess and indicated that the effect of structure can either facilitate or impede the onset of flow liquefaction depending on the state of the soil, termed as the state-dependent flow instability. Such a state-dependency is mainly attributed to the offset of critical state lines (CSL) between the intact and reconstituted loess samples in the $e:\ln p'$ plane. The robust compressive response of intact loess can result in a higher state parameter, and thus higher liquefaction susceptibility. With the improved understanding on the flow behaviors of loess, the failure mechanism of loess flowslides is revisited.

Constitutive models can evaluate volumetric responses induced by shearing, and as a result, provides insights into the development of flow instability or flowslides from a mechanical perspective of soil behavior (e.g. di Prisco et al. 1995). For example, Buscarnera and Whittle (2012) conducted a back-analyze of the Nerlerk berm slide by using the MIT-S1 model and indicated that flow liquefaction may be triggered at different depths, where intense contractive behaviors were found.

The main objectives of this study are: 1) to analyze the flowslides in HFT by comparing the flow instability of intact and reconstituted loess, and 2) to conduct a pilot study to explore flow susceptibility of loess at different states and loading conditions by constitutive modeling.

2 RETROGRESSIVE FLOWSLIDES

2.1 Study area

Heifangtai terrace is an arid loess terrace (area: ~12 km^2) of the Yellow River in the loess plateau of China (see Fig. 1); it consists of the Malan silty loess (thickness: 30 – 50 m), clay (3 – 20 m), and gravel (1 – 10 m) in sequence. The bedrock comprises sandstone with mudstone partings and the bedding plane dipping 135°∠11°. The thickness of the exposed bedrock is greater than 70 m. The average annual precipitation and evaporation are 287.6 mm and 1600 mm, respectively (Zhou 2012). Local inhabitants were re-settled in HFT in the 1960s. Agricultural irrigation was started on the terrace surface by pumping water from the adjacent Yellow River, covering an area of 7.5 km^2 (exceeding 83% of the surface area), with an annual water consumption of 6×10^6 – 8×10^6 m^3.

Peng et al. (2018) analyzed the landslides in HFT and divided them into 5 types distributed in 7 different sections. The failure modes characterize the landslide types, which mainly depend on the angle between the principle sliding direction of the landslide and the bedrock dip. Most loess flowslides concentrate in Sections 2, 5, and 7 (Fig. 1).

Sub-vertical joints are observed in the loess layer which provides preferential paths for groundwater recharge. The apparent spring lines are visible at the bedrock slope along the edge of the terrace, with groundwater seepage at and near the bottom of the loess layer. Land subsidence (> 1 m) was found at several locations in HFT in the early 1980s (Derbyshire et al. 1995). There is no prior knowledge of the groundwater status before irrigation.

2.2 Field observation

As the end of 2019, 21 loess flowslides are found in HFT, with the reach angle ranging from 10°-37° (average 30°). The loess flowslides in HFT typically form a semi-circular scarp, with conchoidal tensile cracks near the crest due to unloading following a landslide event. Field data indicated that the openings of the tensile cracks range from 1 cm to over 100 cm as they approach the crown of the landslide; the openings typically exceed 20 cm with visible vertical surface offsets.

Figure 1. Landslide distribution along the margin of the Heifangtai terrace (HFT) showing 7 sections that are dominated by different types of landslide. Locations of the DC#2 and DC#3 flowslides are shown.

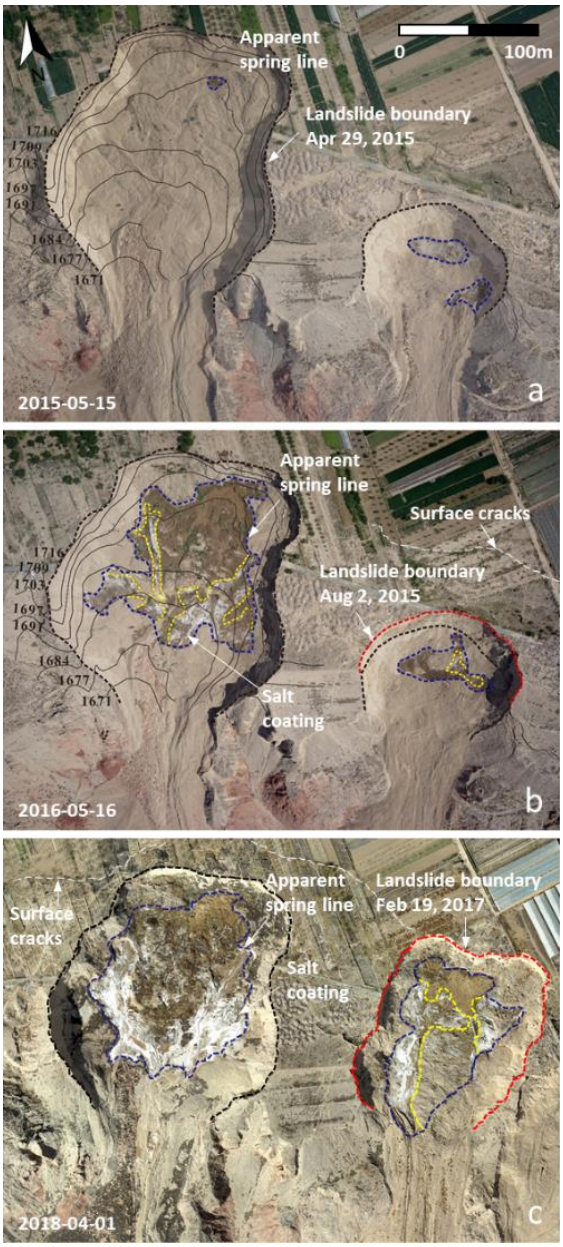

Figure 2. The consecutive failures of the DC#3 (right) and the DC#2 (left) flowslides showing the displaced material near landslide scarp with salt coating and surface runoff.

Irrigating water infiltrates through the sub-vertical joints to the basal zone of the overlying loess layer in HFT (e.g. Zeng et al. 2016). With the increasing area of irrigation, a groundwater dome started to build up, resulting in flow from the center towards the edge. Groundwater discharge is seen on the slope surface, forming the apparent spring line above the impermeable clay layer. Surface runoff results in erosion and deposits a salt coating at the displaced material of landslides. The salt coatings are the results of leaching, as the groundwater dissolves the soluble salts in the Malan loess in HFT (Derbyshire 2001); such a process softens the lower part of the layer by decementation and redistribution of the particles.

Landslides have resulted in pronounced slope retreat along the margin of HFT at an estimated rate of 0.024 km^2/yr (Qi et al. 2018), which is about 3% annual depletion of the terrace. The slope retreat can be demonstrated by the landform changes caused by the DC#3 loess flowslide (Fig. 2). The aerial images between 2015 and 2018 present two consecutive failures of DC#3 of different sizes. The small-scale localized failure occurred on Aug 2, 2015 at the scarp of a previous failure; it is followed by a large-scale flowslide on Feb 19, 2017, developed behind the same scarp. Such a failure process represents the typical sequential failure of a flowslide in HFT.

The field monitoring results of the DC#2 loess flowslide is discussed in Qi et al. (2018). Two failures were observed within 4 hrs; the first appeared to be a more localized small-scale failure while the second was a flowslide. Both failures developed at the same scarp and resulted in a retreat of 130 m. The markers placed behind the scarp showed some cumulative displacement with small increments within three months prior to the failure occurred on Apr 29, 2015 (Fig. 2a). Field data showed no deformation between the first failure and at least 2 hrs prior to the second failure, i.e. the flowslide. The estimated volume of the flowslide is 32.4 × 10^4 m^3 with a maximum runout distance of 789 m.

2.3 Failure process and mechanism

The elevation of the apparent spring line on the top of the displaced material (i.e. bottom of the scarp) is at least 10 m higher than the flanks of the flowslide. It is postulated that such an elevation difference increases over time after a flowslide, as exemplified by the evolution of the apparent spring line in Figure 2.

Qi et al. (2018) proposed a failure mechanism for the flowslides in HFT; it indicated a two-stage failure process involving a small-scale localized failure and a subsequent large-scale long-runout diffuse failure (i.e. flowslide). Both failures developed behind the same scarp. Such a failure mechanism involves a localized hydraulic gradient induced by the morphology of the preceding failure which results in groundwater convergence at the newly established scarp.

The first localized failure may be attributed to the strain-softening of the base of the loess layer due to groundwater; the saturated loess is ready to deform under overburden stress. The displaced materials of the first failure impede the existing seepage on the slope surface, while increasing the localized hydraulic gradient. At this stage, pore-water pressure is built up below the displaced material of the first failure; the soil system is essentially transforming from a drained to an undrained loading condition. As deformation at the crown continues due to the increasing groundwater level, a small axial displacement can induce liquefaction under monotonic loading and result in a liquefied movement of loess. As the flowslide occurs, groundwater converges with slope deformation, and thus by its very nature a new flowslide is likely to follow.

There is no unanimous agreement on the mechanism of flow-like landslides; it is largely ascribed to flow instability in soils. The more widely accepted hypothesis for such an instability process involves pore pressure response (e.g. Iverson 1997, 2012, Hungr and Evans 2004). Although the proposed failure mechanism explains the important role of

groundwater dynamics to the development of the flowslide, the flow instability of loess is not fully understood.

3 EXPERIMENTAL RESULTS

Liu et al. (2019) discussed the results of isotropically consolidated undrained tests (CIU) on the HFT loess. The loess samples were recovered at the scarp of a flowslide in HFT at a depth of 20 m. The sampling depth was selected to be close to the saturated base of the loess layer, with no prior invasion of the groundwater table. Block samples were retrieved and stored in split PVC containers. Index properties of the sample are shown in Table 1.

Table 1. Index properties of the natural HFT loess sample

G_S	e_0	ρ_d (kg/m^3)	w (%)	w_P (%)	w_L (%)
2.69	0.86-0.89	1380	8	17.5	26.8

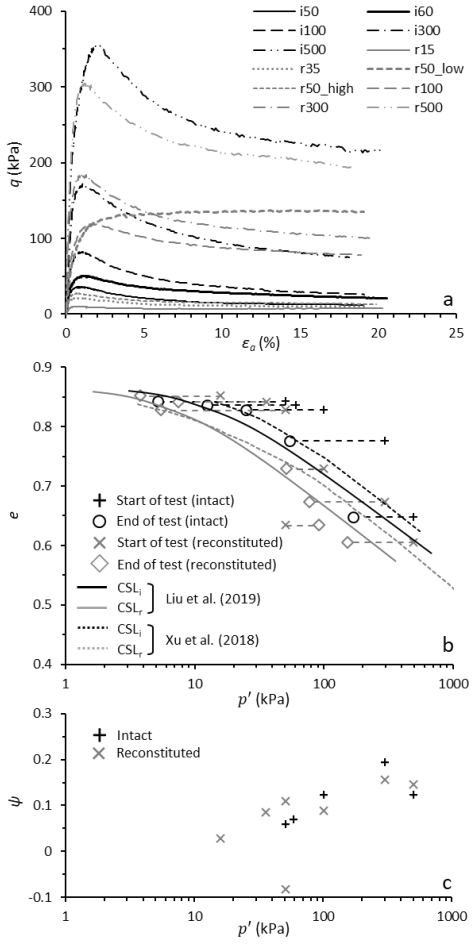

Figure 3. The stress-strain behaviors and the CSLs of the intact and reconstituted specimens of the HFT loess (after Liu et al. 2019): (a) undrained shear stress and axial strain responses; (b) the CSLs and the start-to-end points of the tests; and (c) the state parameters.

The reconstituted specimen was derived from the intact samples by abrading them with sandpaper and prepared by wet compaction at w = 10%, to achieve the initial void ratio of 0.771 – 0.982.

The CIU results of intact and reconstituted specimens showed a strong contractive tendency with intense strain-softening behaviors and sharp increases of pore pressure (Fig. 3a). The results indicated an offset between CSLs of the intact and reconstituted specimens (Fig. 3b). The intact specimens typically located further right of the CSL than the reconstituted samples at the same stress level with similar e_0, which is attributed to the effect of structure that resulted in more robust compressive responses during consolidation, and thus a higher void ratio at the beginning of shearing for intact specimens. For CSL at stress above 100 kPa, the effect of structure is likely to cause a larger difference in e_c between intact and reconstituted specimens with the same e_0, which results in a higher susceptibility to instability for intact specimens with a higher state parameter. However, it is postulated that such an effect may be less pronounced by further increasing p_0', as ψ appears to be reduced for intact specimens at p_0' > 300 kPa (Fig. 3c).

The intact loess is more susceptible to flow instability at lower stress levels, ranging from p_0' = 100 – 300 kPa, due to the effect of structure. Such a finding can be reflected in the field; the apex of the apparent spring line at the deposit of flowslides is typically found to be about 20 m in depth prior to a new failure, corresponding to the p_0' of about 200 kPa at the beginning of shearing for intact loess. However, it is not practical to prepare the specimens with the same state parameter in order to compare the undrained behaviors.

4 NUMERICAL INVESTIGATION

The constitutive understanding of flow instability of the HFT silty loess is based on the NorSand model (Jefferies 1993). NorSand model is a generalized CSSM-based constitutive model for particulate materials, which can provide a means to assess the development of flow liquefaction of sands or silts. The differences of flow behaviors between intact and reconstituted loess at the same ψ is modelled to study the effect of structure on flow instability. The implications of the drained-to-undrained transition is discussed in the context flowslide initiation.

4.1 Calibration of NorSand

The calibration of the NorSand model for the silty loess has required a number of approximations. A set of curved CSL's are idealized to fit CSL$_i$ and CSL$_r$ (Liu et al. 2019). The effect of structure of intact loess is replicated by introducing an overconsolidation ratio (OCR) of 1.6, and it is assumed that OCR reduces to unity for reconstituted loess. The material parameters of NorSand model are calibrated for the intact and reconstituted states separately. The model parameters are listed in Table 2.

Input parameters are obtained by fitting low-pressure data for intact and reconstituted loess. Figure 4 compares the computed and measured stress-strain behaviors and

effective stress paths for HFT loess in CIU tests. Test i50 (Fig. 3) is used for calibration and test i100 confirms the selected parameter for intact specimen. Tests r35 and r50 are used for calibration and test r100 confirms the selected parameter for reconstituted specimen. The model captures the first-order features in the measured behaviors. While the model underestimates the peak shear strength for p_0' = 100 kPa, it appears to give an adequate description of the post-peak strength.

Table 2. Summary of NorSand model parameters

Parameter or Symbol	Definition	Intact loess	Recon loess
Γ	Void ratio intercept at unit pressure	0.89	0.88
λ_{10}	Slope gradient of the CSL	Curved	Curved
M_{tc}	Critical state stress ratio	1.36	1.36
N	Volumetric coupling coefficient	0.3	0.3
χ_{tc}	State-dilatancy coefficient	3.5	3.5
H	Plastic hardening modulus	~150	~100
I_r	Elastic modulus (=G_0/p_0)	~110	~70
ν	Poisson's ratio	0.2	0.2

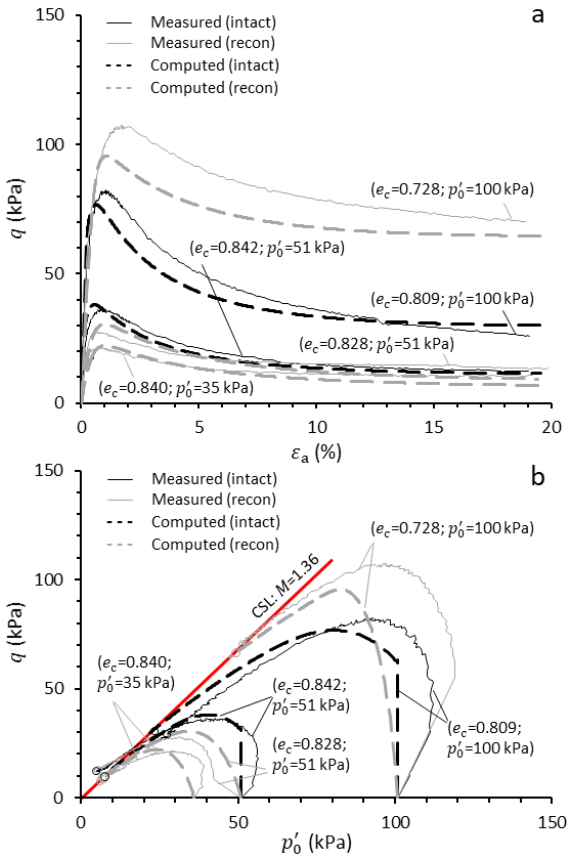

Figure 4. Calibration of undrained behaviors of intact and reconstituted HFT loess: (a) stress-strain responses; and (b) undrained loading paths.

Jefferies et al. (2012) illustrated that the peak undrained shear strength and strain-softening is strongly dependent on the elastic stiffness and plastic hardening of sand in light of NorSand model. Similar observations are made for HFT silty loess; variations of I_r and H can considerably alter the stress-strain responses. Increasing I_r or H can result in a higher pore-water pressure as larger elastic or plastic strain is developed to compensate for shear-induced contraction under constant volume.

4.2 Effect of structure on flow instability

The effect of structure of loess can be quantitively analyzed by setting the state parameters of intact and reconstituted specimens to be equal in the model, assuming that the reconstituted sample precludes the effect of structure.

Figure 5 compares the modeled stress-strain behaviors and the effective stress paths of the HFT loess at its intact and reconstituted states with the same state parameter. The experimental results of intact loess are also presented for comparison. It is clear that the computed peak strength of the intact specimen, all other factors being equal, is higher than that of the reconstituted specimen. However, the post-peak strength is lower for intact specimen. Figure 5 also shows a clear shift of the instability loci (IL) from the intact to the reconstituted effective stress paths, indicating a decrease of instability region in the reconstituted loess. The post-peak shear strength of the intact specimen is about 0.5 of the reconstituted specimen for the same ψ under the same p_0'.

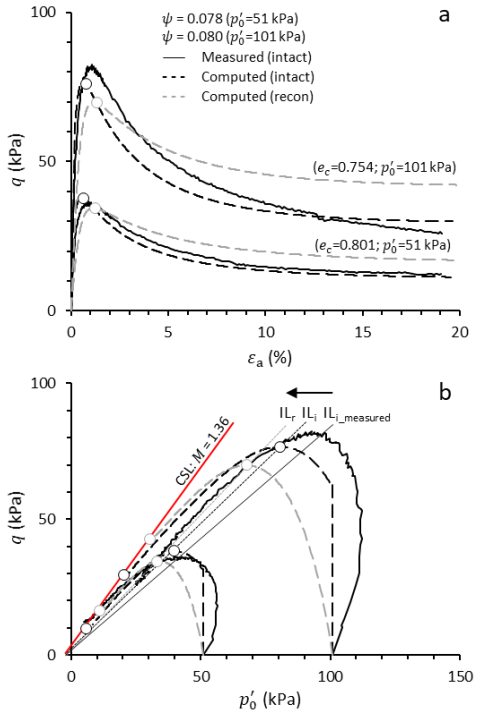

Figure 5. The computed undrained behaviors of intact and reconstituted HFT loess at the same state parameters: (a) stress-strain responses; and (b) undrained loading paths.

4.3 Triggering of flowslides

In the context of flowslides, as flow instability occurs, the drastically reduced stress and excess pore-water pressure leads to a 'flow-like' movement as rapid development of large strain is required for maintaining equilibrium when the shear strength required is greater than can be mobilized in the soil.

In the case of the flowslides in HFT, the groundwater movement behind the scarp may further contribute to the instability by producing a drained-to-undrained transition, which is of direct interest to the development of flow-like landslides. di Prisco (1995) presented the sharp reduction of strength by switching the load from drained to undrained conditions. Jefferies and Been (2015) illustrated that rapid reduction of strength by differing the k_0 values to change the ratio of drained to undrained portions of the loading path.

By following the approach of Jefferies and Been (2015), Figure 6 presents a simplified illustration on the effects of drained-to-undrained transition along the loading paths on the instability of intact loess, in which k_0 represents the end of a drained loading path and the onset of undrained loading path. The OCR in Figures 4 and 5 is not applied here. The undrained strength increases with decreasing k_0 due to higher initial shear stresses (Fig. 6); however, the strength declines immediately after k_0 > 0.5 when altering the loading path from drained to undrained in the model. No apparent effect of p_0' was found on the drainage transition.

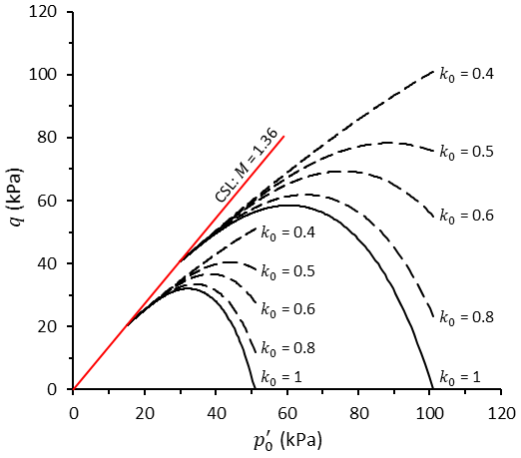

Figure 6. Computed flow liquefaction for different drained-to-undrained loading paths.

In the actual field, this drained-to-undrained transition can be achieved by impeding the surface seepage due to the first-stage small-scale slope failure. Depending on the initial *in situ* shear stress and the thickness/volume of the deposits, the drained-to-undrained loading path may change, and thus the mobilized shear stress at failure (or the required shear perturbation) may change; such a process can be indicated by field observations where the period between the first-stage small-scale failure and the second-stage flowslide varies from hours to years.

5 DISCUSSION AND CONCLUSION

The failure process and mechanism of the loess flowslides in HFT is revisited with the support of CIU test data on the intact and reconstituted loess. Based on the experimental results, the effect of structure can either facilitate or impede the onset of flow instability of loess, depending on the state of the soil, and therefore understanding the relative position between the state of a loess and its CSL aids in analyzing flow instability and flowslide occurrence.

A preliminary constitutive understanding on the flow instability of loess is gained by computing the undrained behaviors of intact and reconstituted loess with the NorSand model. The model indicated that the development of pore-water pressure is largely affected by the elastic and plastic moduli of loess. While the current combination of I_r and H has yielded reasonable representations for stress-strain behaviors, the resultant small-strain stiffness G_0 are found to be 5.5 MPa for intact and 3.5 MPa for reconstituted loess specimens at p_0' = 51 kPa, respectively, Such a finding is substantially lower than the corresponding G_0 of 50 MPa and 20 MPa, as reported by Zuo et al. (2020).

The undrained loading paths of intact and reconstituted states with the same state parameter is compared with NorSand model, as such an identical pair of intact and reconstituted specimens is practically impossible to be produced in the CIU tests. The results show that the structure of loess facilitates the development flow instability in the stress range of p_0' = 50-100 kPa, with a post-peak strength of about half of that of its reconstituted state.

The drained-to-undrained transition found in the field is discussed in light of the computed results by simulating a drained-to-undrained transition along the loading path of intact loess. The results of such a transition, achieved by changing k_0, have shown a rapid reduction of strength by switching drained loading to undrained loading, especially with more shearing along the drained loading path. Such a finding explains the varying period between the first small-scale failure and the second large-scale flowslide, as seen in many loess flowslides in HFT.

ACKNOWLEDGMENTS

The authors gratefully acknowledge the financial supports of the Elizabeth and Bill Higginbotham Professorship at the Georgia Institute of Technology and the National Natural Science Foundation of China (grant No. 41790445) at the Chengdu University of Technology. The authors are grateful to Mike Jefferies for providing the NorSand model and for his comments about the model.

REFERENCES

Barden, L., McGown, A., and Collins, K. 1973. The collapse mechanism in partly saturated soil. Engineering Geology, **7**(1): 49–60.

Buscarnera, G., and Whittle, A.J. 2012. Constitutive modelling approach for evaluating the triggering of flow slides. Canadian Geotechnical Journal, **49**(5): 499–511. NRC Research Press.

Carrera, A., Coop, M., and Lancellotta, R. 2011. Influence of grading on the mechanical behaviour of Stava tailings. Géotechnique, **61**(11): 935–946. doi:10.1680/geot.9.P.009.

Delage, P., Audiguier, M., Cui, Y.-J., and Howat, M.D. 1996. Microstructure of a compacted silt. Canadian Geotechnical Journal, **33**(1): 150–158. NRC Research Press.

Derbyshire, E. 2001. Geological hazards in loess terrain, with particular reference to the loess regions of China. Earth-Science Reviews, **54**(1–3): 231–260. doi:10.1016/S0012-8252(01)00050-2.

Derbyshire, E., and Mellors, T.W. 1988. Geological and geotechnical characteristics of some loess and loessic soils from China and Britain: A comparison. Engineering Geology, **25**(2–4): 135–175. doi:10.1016/0013-7952(88)90024-5.

Derbyshire, E., Meng, X., Wang, J., Zhou, Z., and Li., B. 1995. Collapsible loess on the loess plateau of China. *In* Genesis and Properties of Collapsible Soils. Springer Netherlands. pp. 267–293.

Fan, X., Xu, Q., Scaringi, G., Li, S., and Peng, D. 2017. A chemo-mechanical insight into the failure mechanism of frequently occurred landslides in the Loess Plateau, Gansu Province, China. Engineering Geology, **228**(June): 337–345. doi:10.1016/j.enggeo.2017.09.003.

Hungr, O., and Evans, S.G. 2004. Entrainment of debris in rock avalanches: an analysis of a long run-out mechanism. Geological Society of America Bulletin, **116**(9–10): 1240–1252. Geological Society of America.

Iverson, R.M. 1997. The Physics of Debris Flows. Reviews of geophysics, **35**(3): 245–296.

Iverson, R.M. 2012. Elementary theory of bed-sediment entrainment by debris flows and avalanches. Journal of Geophysical Research: Earth Surface, **117**(F3).

Jefferies, M. 1993. Nor-Sand: a simle critical state model for sand. Géotechnique, **43**(1): 91–103. Thomas Telford Ltd.

Jefferies, M., and Been, K. 2015. Soil liquefaction: a critical state approach. *In* 2nd edition. CRC press.

Jefferies, M., Been, K., and Olivera, R. 2012. Discussion of "Evaluation of static liquefaction potential of silty sand slopes." Canadian Geotechnical Journal, **49**(6): 746–750. NRC Research Press.

Jiang, M., Hu, H., and Liu, F. 2012. Summary of collapsible behaviour of artificially structured loess in oedometer and triaxial wetting tests. Canadian Geotechnical Journal, **49**(10): 1147–1157. doi:10.1139/t2012-075.

Leng, Y., Peng, J., Wang, Q., Meng, Z., and Huang, W. 2018. A fluidized landslide occurred in the Loess Plateau: A study on loess landslide in South Jingyang tableland. Engineering Geology, **236**(4): 129–136. doi:10.1016/j.enggeo.2017.05.006.

Liu, F., Xu, Q., Zhang, Y., Frost, J.D., and Zhang, X. 2019. State-dependent flow instability of a silty loess. Géotechnique Letters, **9**(1): 22–27.

Milodowski, A.E., Northmore, K.J., Kemp, S.J., Entwisle, D.C., Gunn, D.A., Jackson, P.D., Boardman, D.I., Zoumpakis, A., Rogers, C.D.F., Dixon, N., Jefferson, I., Smalley, I.J., and Clarke, M. 2015. The mineralogy and fabric of 'Brickearths' in Kent, UK and their relationship to engineering behaviour. Bulletin of Engineering Geology and the Environment, **74**(4): 1187–1211. doi:10.1007/s10064-014-0694-5.

Peng, D., Xu, Q., Liu, F., He, Y., Zhang, S., Qi, X., Zhao, K., and Zhang, X. 2018. Distribution and failure modes of the landslides in Heitai terrace, China. Engineering Geology, **236**(June 2016): 97–110. Elsevier. doi:10.1016/j.enggeo.2017.09.016.

di Prisco, C., Matiotti, R., and Nova, R. 1995. Theoretical investigation of the undrained stability of shallow submerged slopes. Géotechnique, **45**(3): 479–496. Thomas Telford Ltd.

Pye, K. 1995. The nature, origin and accumulation of loess. Quaternary Science Reviews, **14**(7–8): 653–667. doi:10.1016/0277-3791(95)00047-X.

Qi, X., Xu, Q., and Liu, F. 2018. Analysis of retrogressive loess flowslides in Heifangtai, China. Engineering Geology, **236**: 119–128. doi:10.1016/j.enggeo.2017.08.028.

Smalley, I.J., Mavlyanova, N.G., Rakhmatullaev, K.L., Shermatov, M.S., Machalett, B., O'Hara Dhand, K., and Jefferson, I.F. 2006. The formation of loess deposits in the Tashkent region and parts of Central Asia; and problems with irrigation, hydrocollapse and soil erosion. Quaternary International, **152**: 59–69. doi:10.1016/j.quaint.2006.02.018.

Xu, L., Coop, M.R., Zhang, M.S., and Wang, G. 2018. The mechanics of a saturated silty loess and implications for landslides. Engineering Geology, **236**(5): 29–42.

Zeng, R.Q., Meng, X.M., Zhang, F.Y., Wang, S.Y., Cui, Z.J., Zhang, M.S., Zhang, Y., and Chen, G. 2016. Characterizing hydrological processes on loess slopes using electrical resistivity tomography - A case study of the Heifangtai Terrace, Northwest China. Journal of Hydrology, **541**: 742–753. Elsevier B.V. doi:10.1016/j.jhydrol.2016.07.033.

Zhang, F., and Wang, G. 2018. Effect of irrigation-induced densification on the post-failure behavior of loess flowslides occurring on the Heifangtai area, Gansu, China. Engineering Geology, **236**: 111–118.

Zhou, Y.F. 2012. Study on Landslides in Loess Slope due to Infiltration. University of Hong Kong.

Zhou, Y.F., Tham, L.G., Yan, W.M., Dai, F.C., and Xu, L. 2014. Laboratory study on soil behavior in loess slope subjected to infiltration. Engineering Geology, **183**: 31–38. doi:10.1016/j.enggeo.2014.09.010.

Zuo, L., Xu, L., Baudet, B.A., Gao, C., and Huang, C. 2020. The structure degradation of a silty loess induced by long-term water seepage. Engineering Geology,: 105634. Elsevier.